A model-based approach to battery selection for truck onboard fuel cell-based APU in an anti-idling application

Boštjan Pregelj, Darko Vrečko, Janko Petrovčič, Vladimir Jovan, Gregor Dolanc

bostjan.pregelj@ijs.si;

Jozef Stefan Institute, Jamova 39, 1000 Ljubljana, Slovenia

Abstract: The paper presents a model-based approach to supporting battery selection for a fuel cell (FC)-based auxiliary power unit (APU). It is introduced to a case study of electrical power production and consumption management in a truck anti-idling application of a diesel-powered FC-based APU, a system under development in FCGEN, a FCH JU European project of the FP7 program. With fuel cell and related technologies increasingly competing with others in the market, they need to form complete systems with matching and well-balanced components to enable using the technology to its best. Within the whole system, the battery, serving as an energy buffer, represents a medium-cost element, but it affects the operating parameters importantly. Within the scope of this study, a purpose-oriented model of the diesel powered FC-based system is developed together with a realistic load scenario for the comparison of three batteries. The battery size and type are investigated and discussed in the light of the simulation results.

Key words: battery selection; truck onboard APU; efficiency model; load study fuel cells; fuel processor

1 Introduction

Fuel cells with a membrane made from a polymer material, known as *Polymer Electrolyte Membrane fuel cells* (PEM FC), are a clean and efficient source of electrical energy [1][2], [3], [4]. Other advantages are their low operating temperatures, high power density, and silent operation [5], [6]. Nowadays, as fuel cell (FC) technologies are getting closer to everyday use, they are increasingly competing with other technologies on the market for both stationary [7], mobile [8] and portable [9]applications. This requires several aspects of such systems to be optimized; namely, their economics, reliability, and sustainability [2], [6]. Therefore, the system integrator must choose the supporting components correctly, tune the control accordingly, and possibly implement additional diagnostic methods [10], [11] to exploit each component optimally and allow optimal operation of such a power unit as a whole. Still, FC systems are mainly produced in a small series and, as a result, the supporting subsystems are rarely properly matched to the FC stack and reformer-rated power. The consequences of inappropriate dimensioning of system parts (e.g., pumps, blowers, fans, batteries, etc.) may result in higher prices, lower efficiency, and shorter lifetimes of the overall systems.

Recently the niche market for FC-based onboard auxiliary power generation units (APU) has been making big steps towards acquiring a presence in the wider market [12], [13], with APUs

often also including the fuel processor (FP) [14], [15]. There is an interest in such products in the vehicle market for trucks, caravans, and busses, and in the nautical field for small to mid-sized yachts and sailboats, providing that a decent price, reliability, and a sufficient lifetime are offered. Among the above, there is a field of truck anti-idling APU applications, where recent interest and a development push has come about due to the negative effects of idling [16] and a tightened regulative environment [17], [18]. The fuel cell-based onboard APUs [19], [20] run at higher efficiency and have much lower emissions. Market analyses [21], as well as possible use and impact investigations [22], have been done already and several research projects (e.g., FCGEN [23], DESTA [24]), etc. have been financed to overcome further obstacles to commercialization and to demonstrate their use.

One important performance and price-influencing APU component is the battery. Due to thermo-chemical processes, the FC systems and the fuel reformers even more so belong to slowly responsive energy sources and such APUs therefore predominantly require an energy buffer to cover the load transients [7], [8]. Yet, an energy storage element places limitations on the energy and power capacities, which dictates its price. Therefore, the selection of an appropriate battery for such a system is a delicate task, requiring experience and insight that can be obtained through experimentation; it is an expensive and time-demanding task, and sometimes it is also difficult to carry out due to operational restrictions. On the other hand, a simulation approach is a good alternative that overcomes most of these issues [8], [26] and enables observation of close to real system behavior to take place in a faster, more convenient, and less expensive way.

In this work we present a model-based approach to supporting decisions about battery selection for an APU system. The concept comprises (i) the efficiency and power models of the main APU components, (ii) the battery models, (iii) the power consumption model, and (iv) the control system. This approach is used to evaluate the three batteries considered within the FCGEN project: the lead-acid starter and traction batteries, and the lithium battery. There the task to select an appropriate battery was a part of the APU process design phase – before the components were built and real process data was available to verify the model precisely. Therefore the results are not expected to yield precise numbers but to give insight and better background for well informed decision on battery to be used.

To enable a sensible evaluation to take place, typical loads were identified and their usage profiles for an anti-idling truck onboard application were specified. The resulting overall load profile was confirmed by the truck-producing company. Additionally, an advanced control algorithm from previous work [27] was upgraded to comply with the components' limitations and to further optimize the overall APU performance. The simulations are used to generate data on the basis of which the advantages and disadvantages of each APU-battery assembly are discussed.

The paper first presents the relevant model of the APU, consisting of the lumped component models of a reformer, a stack, a DC/DC converter, and parasitic loads and batteries in three

variants. Following the description of the advanced-level control system structure and functions, the related loads and the profiles of the truck's onboard application are presented. The batteries are evaluated in the simulation using the described model and load profile. The findings of the comparison are summarized and there is a discussion relating to overall efficiency, battery price, and aspects of practical use.

2 The APU model

The diesel-powered FC-based APU with 3 kW net electrical output power, developed within the FCGEN project, is a complex system consisting of several reactors, where various chemical reactions take place. Reactor masses impose spatial temperature distributions and high order responses. Furthermore, the reformate chain connecting all the reactors means that each phenomena propagates through downstream reactors, which imposes tight control constraints. Thus the challenges are also in succeeding to manage and control the operation of the complete system reliably and efficiently. The APU process scheme is shown in Figure 1.

Due to complex and slow dynamics, imposed predominantly by fuel processor, the battery is required to compensate the APU power excess/shortage in relation to load demand.

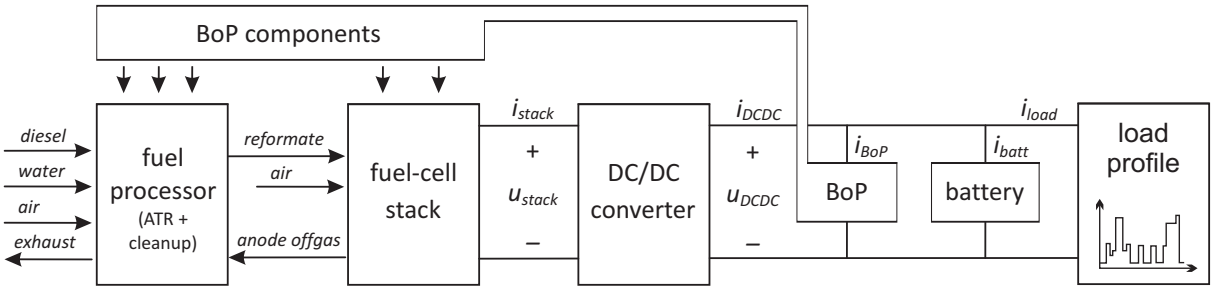

Figure 1. The APU process scheme.

However, the focus of the analysis presented here is on the APU power, battery and load-related phenomena and has a macroscopic nature. It was required to help decide the most suitable battery to use with the APU in advance – during the APU design phase. This has two implications. First, due to macroscopic nature of the study the use of detailed dynamic process models of APU components does not bring significant benefit, but complicates the modeling and increases the model complexity over the desired level. Therefore, lumped models are used, which include only the most dominant time dynamics of some components and their characteristics. Second, the model is based on preliminary component characteristics provided by component producers/developers.

The component degradation is not taken into account in this work. The degrading phenomena are prevented to the highest possible degree by the means of operation-optimized control strategy and set-points selected in the safe area of operation. E.g. the starvation possibility is reduced by the stack blower controlled to the appropriate lambda and by means of stack current rate constraints, implemented through the DCDC converter control that allow the FP to

follow with preparation of the requested reformate flow. During these transients the battery takes the load until the stack current gradually reaches an adequate level.

The model comprises the following:

- Fuel processor (FP)
- Fuel cell stack (FC)
- Power converter (DCDC)
- Battery.

To run the model correctly the following load parameters also have to be defined:

- Daily load profile
- Power consumption characteristics of the balance of plant (BoP) components
- Duration and power consumption of APU startup and shutdown procedures.

All the listed components are described in the following sections.

2.1 The fuel processor model

The fuel processor consists of several reactors: the autothermal diesel reformer (ATR) [28], [29] the sulphur and CO cleanup reactors, and the catalytic burner after the FC stack. For reforming three components are required: air, fuel and steam. Air and diesel are provided directly by blower and high-pressure pump while the water is fed through and evaporated in the catalytic after burner, where the unused hydrogen from the stack anode off-gas is burned. Opposite to the steam reformer, in the ATR a combination of exothermic partial oxidation and endothermic steam reforming (to syngas - H_2 and CO) take place. The heat released by the partial oxidation is used to maintain the endothermic steam reforming. The molar O_2/C ratio (air-to-diesel) governs the extent to which these both reactions can proceed. E.g., by increasing the molar O_2/C ratio the partial oxidation is favored.

For the purpose of this investigation, the FP has been modeled with the efficiency characteristics, load dynamic constraints, and min/max thermal load limits. Considering the reformer, FC stack, and power converter efficiencies and the stack H_2 utilization rate, the FP operating range relates to 2.3 to 4.5 kW stack output power (i.e., 50 A to 150 A of stack output current). For a better representation, the reformer efficiency as well as other characteristics in this work are given in relation to stack output current. The FP efficiency is the ratio between the powers of the reformate flow to FC and the diesel flow to ATR. It is slightly lower at part load, as due to heat-loses the ATR has to be operated with more air (a higher O_2/C ratio) to keep the catalyst at optimal operating temperature ensuring good diesel conversion, which is essential for health and longevity of the fuel cell stack as well as other reactors. This characteristic is shown in Figure 2 and the FP dynamic constraints were set and recalculated to a stack output power with a value of 1kW/min.

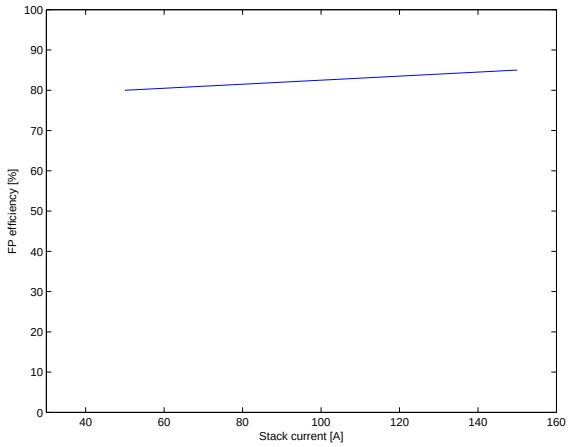

Figure 2. Fuel processor efficiency characteristics in relation to stack output current.

2.2 The fuel cell stack model

The fuel cell stack is a water-cooled 50-cell low-temperature PEM type. It uses the reformate from the ATR , with CO removed by water-gas-shift (WGS) and preferential-oxidation (PROX) reactors, and air supplied by air blower, controlled to adequate λ value to ensure safe and efficient operation. It has been modeled with polarization and efficiency curves (shown in Figures 3 and 4, respectively) given by the manufacturer [30]. The presented efficiency curve also takes into account the hydrogen utilization in the stack with is artificially lowered by reducing stack current via DCDC converter to values of 71% and 80% at 50 and 150 A, respectively. The unutilized hydrogen is burned in a catalytic after burner to generate the steam required by the ATR. Due to heat losses and conditions for stable steam production relatively more energy is required at part load resulting in required lower H_2 utilization.

Since the FC stack is capable of much faster load transitions than the fuel processor, no further rate constraints have been introduced to the model. In the described APU application, the upper stack operating point is at approximately 150 A.

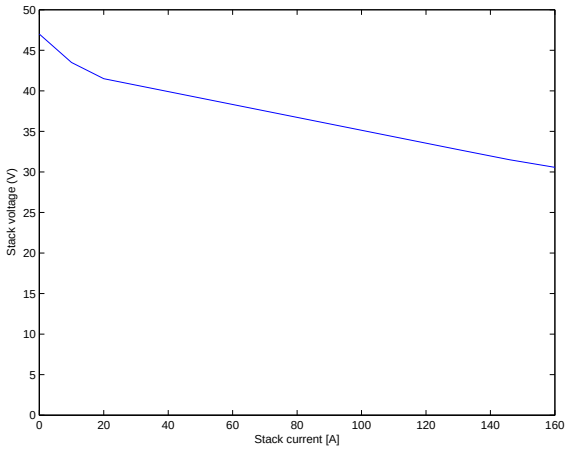

Figure 3. Fuel cell stack voltage as a function of output current; operating range stretches from 0 to 150 A [30].

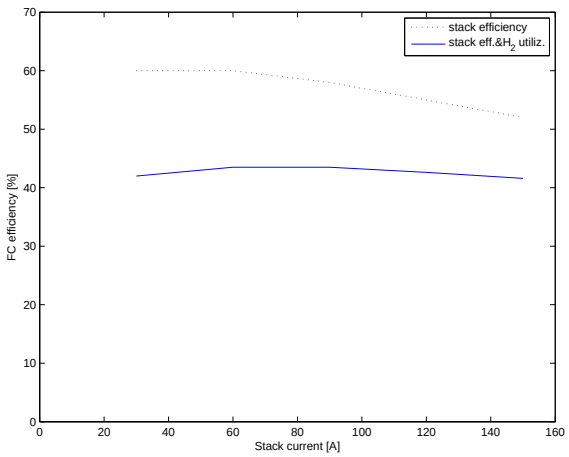

Figure 4. Fuel cell efficiency (dotted line) and the stack efficiency (also considering stack H_2 utilization) (full line) in relation to output current [30].

2.3 The power converter model

The power converter (DC/DC) has been modeled as a voltage converter using the *d*-parameter for voltage ratio and a constant 95% operation efficiency. In this case, a step-down (buck) converter is used since the stack voltage (32–48 V) is always higher than the required battery/bus voltage (24–30 V). Due to its much faster dynamics compared to the other components in the system, a lumped model of a DC/DC converter can be used:

$$d = \frac{U_{out}}{U_{in}}; \quad \mu = \frac{P_{out}}{P_{in}} = \frac{I_{out}U_{out}}{I_{in}U_{in}} = \frac{I_{DCDC}U_{batt}}{I_{FC}U_{FC}}, \tag{1}$$

where *d* is the converter duty cycle (0–100%), also representing the output/input voltage ratio (controlled input), and μ is the constant converter efficiency of 95%. *P*, *U,* and *I* represent the power, the voltage, and the current on the stack (*in*) and the battery (*out*) side of the converter.

2.4 The battery model

The batteries investigated in this work have been designed for different purposes and also at different points in time – lead-acid technology that has been exploited for a long time [32], but lithium only within the last decades [34]. Each of these types of battery has advantages and disadvantages, and the purpose of their use may justify the technology selection over the price.

In order not to increase the space and weight of the APU, candidate batteries were selected that could be fitted into one of the present battery compartments onboard the truck. The first was the standard truck 24 V starting battery (SLI) with 220 Ah, the second was a traction battery of the same capacity, and third was a 26 V, 100 Ah, engine-start capable lithium-ion battery. Their operational data are presented in Table 1.

Table 1. Operational data for the considered batteries.

Bat. type	***Lead-acid SLI* [32]**	***Lead-acid traction* [32]**	***Lithium-ion* [33]**
Nom. voltage, capacity	24V, 220 Ah	24V, 220 Ah	26V, 100 Ah
Max. charging current	0.2 C[a] (44 A)	0.2 C (44 A)	1 C or more (100 A)
Recommended discharge current	short 5 C (1200 A) long C/5 (44 A)	C/5 (44 A)	short >10 C (1000 A) long 2–3 C (100 A)
Weight	~65 kg	~130 kg	42 kg (35–45 kg)

[a] C – value of battery capacity in Ah.

This study has a macroscopic nature and has no intent of going in to detailed battery operation analysis. Therefore fast, practical and understandable models have been favored. For comparability with the previous work [27] themodel from the Matlab/Simulink in the SimPowerSystems library [31]was used for modeling the battery. It provides different models for the lead-acid, NiCd, NiMh and Lithium-ion batteries, and offers complete battery behaviour model [31]including losses and current influence . The limitations on charge/discharge currents related to the battery size and type are imposed within the control algorithm.

2.5 The balance of plant components' power consumption

The APU operation is supported by 9 valves, 12 pumps, and 15 compressors/blowers. Some of them run constantly regardless of the APU power level (cooling water pumps), while others follow the operating point. Since the APU reactors dictate specific flows, pressures, and so on, it is difficult to find matching balance of plant (BoP) components. For example some blowers have to have very large operating range to ensure fast startup. Consequently, they are oversized, which in turn significantly reduces the overall APU efficiency. Based on the components' data (blowers, pumps), their power consumption has been estimated to model the real operating situation and the resulting cumulative power was 1.3 kW at 50 A and 1.5 kW at 150 A of stack output power, and linear dependency is assumed between those two points. The relation is presented in Figure 5.

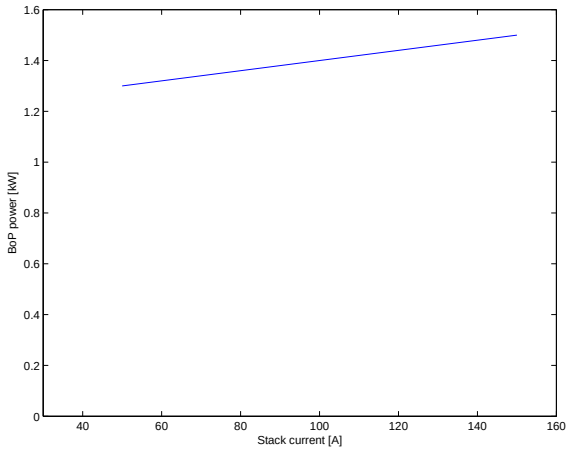

Figure 5. Power consumption of the balance of plant components in relation to stack output current.

2.6 The startup and shutdown procedures

Here, the necessary steps from full shutdown to operation and back are modeled. For operation the fuel processor reactors have to be at certain temperature levels, requiring heat-up and cool-down sequences. From the modeling point of view, two aspects have to be addressed for this study. The first is the time needed to bring the FP reactors to the operating temperature and to cool down at the end, and the second is the electrical power consumed by the BoP components during these stages.

During startup the main power consumers are the ATR (cca. 400 W) and the CAB (cca. 60W) blowers that take the heat from the start-up-burner exhaust and spread it through the fuel-processor reactors to heat all to operating temperatures..,The cumulative power of 0.5 kW and duration of 0.6 hours have been roughly estimated based on required reactor temperatures, reactor masses and start-burner power. During shut-down several cooling components are engaged in specific sequence to clean and safely cool-down the reactors. For this the consumption was estimated to be 0.4 kW and duration to 0.6 hours (as summarized in Table 2). The energy consumption of the BoP components for startup and shutdown was modeled for before and after each APU operation period.

Table 2. The BoP components' power consumption for the APU startup and shutdown phases

Load	Power usage (W)	Up-time est./run (h)	Energy/run (Wh)
Startup	500	0.6	300
Shutdown	400	0.6	240

3 The APU control

3.1 The hierarchic control structure

The control and power management algorithm has to ensure that the APU can provide energy at the declared levels at any time, while maintaining optimal operating points whenever possible and minimizing the number of battery cycles. This is done by hierarchical control shown in Figure 6, which has been further upgraded from the previous work presented in [27]. The *supervisory controller* monitors the APU operation, estimates system states, executes the startup and shutdown sequences and defines the stack current and other flow setpoints for the lower-level *load controller.* The latter controls the BoP components that maintain optimal reactant flows, cool reactors, and so on. Its description (partly provided in [27]) is far beyond the scope of this work and here we will just assume it works appropriately and exploits the components in accordance with their design.

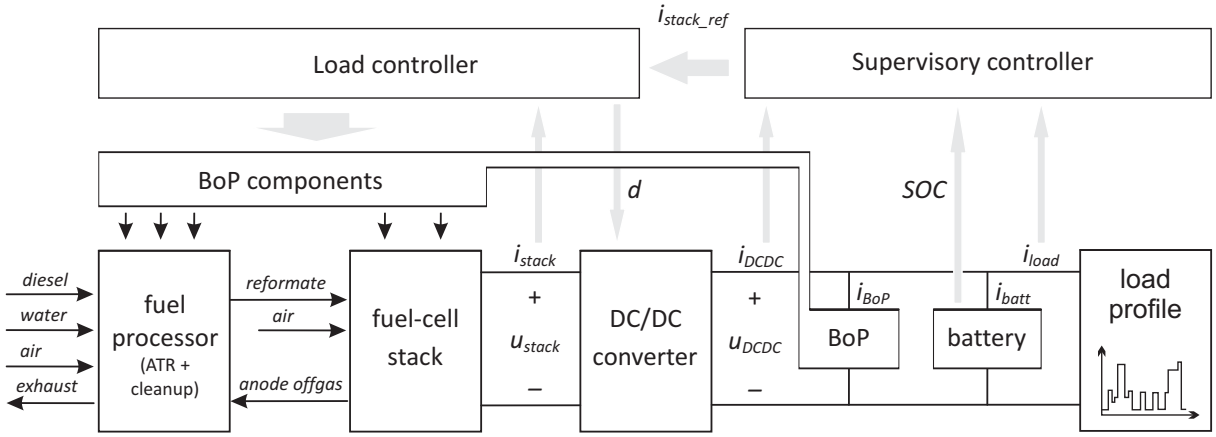

Figure 6. The APU control with the control system scheme (black and grey lines represent physical and control signals, respectively).

The *supervisory controller* has a two-level state machine structure, as shown in Figure 7. At the top there are two main operational states: *ON* and *OFF*. In the *ON* state the system is able to provide power to loads, whereas in the *OFF* state it is completely shut down. Below this there are further two state automata that are active in the main state *ON*. The first, called "*battery control*," has two states and models the battery charging control, and its output (CHG) dictates the operation of the second one. The second, called "*FP/FC*," is composed of four states and governs the FP/FC operation. In the *standby* state the *FP/FC* is stopped and the battery provides power to loads. When the battery has discharged to below the lower state of charge

(SOC) limit, the automaton switches to *startup* state. When the FP/FC startup procedure is done, the system switches to *operation*. There the FP/FC power is controlled to power the loads, while maintaining the battery charging current within the allowed limits (44 A for lead-acid and 100 A for lithium) and varying the FP/FC power level. The FP/FC power level change is always executed via slow ramp that compensates the process dynamic and ensures healthy operation of the fuel processor (good conversion) as well as the stack (no starvation). As the battery is charged to the upper SOC limit, the *shutdown* state is activated, where the system (stack, reactors, piping) is purged and all components are cooled down. After that the automaton switches back to *standby* state. The upper and lower SOC limits are calculated dynamically in a way that also considers the load, as described in following section.

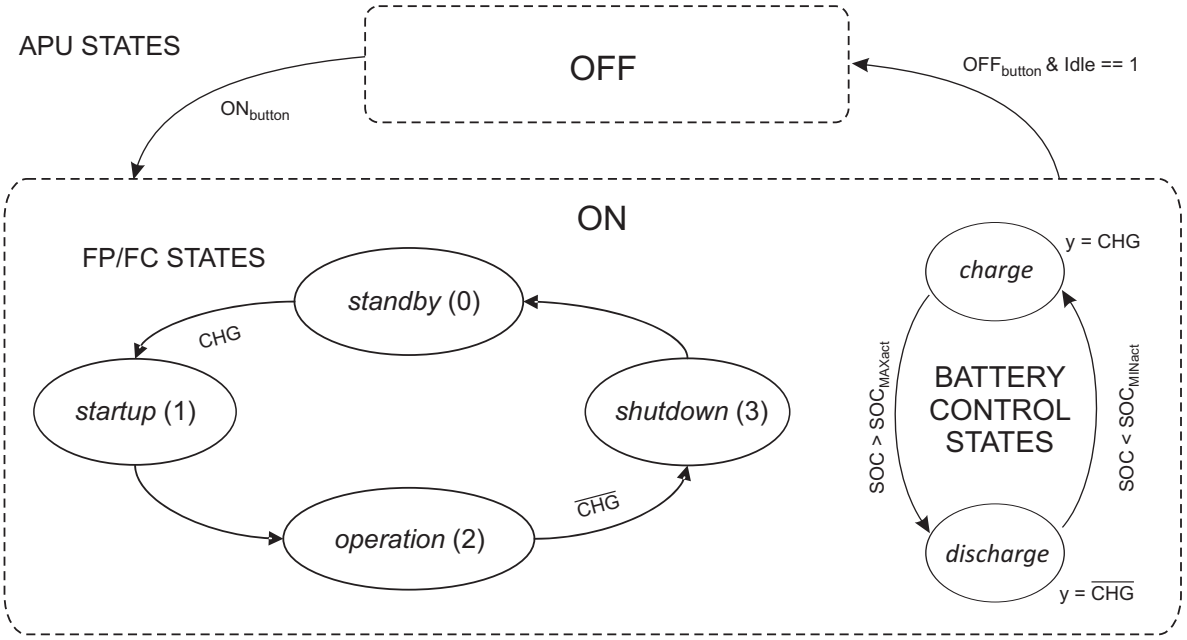

Figure 7. The APU control hierarchy: the main (APU) and the supporting (FP/FC and Battery) control automata.

3.2 The dynamic estimation of the upper and lower SOC thresholds

To optimize the overall APU efficiency we have to maximize its operation time and prevent the battery from depleting or overcharging. Taking into account the APU operating conditions and parameters, this is done by dynamic variation of the actual lower and upper battery SOC thresholds that trigger APU startup and shutdown procedures.

In order not to deplete the battery below its nominal lower SOC limit during the startup, the actual minimal threshold has to be increased above the nominal limit. Based on the short-term average APU load, the power required by the APU during startup, and the startup time, this is estimated by the following equation:

$$SOC_{MINact} = SOC_{MIN} + \left(\frac{P_{start}}{U_{batt_0}} + I_{loadAVG}\right) * \frac{t_{start}}{C_{batt}} * 100\%\,, \qquad (2)$$

where SOC_{MIN} is the lower nominal SOC limit, P_{start} is the startup consumption of the APU BoP components, t_{start} is the startup time, U_{batt_0} is the nominal battery voltage, C_{batt} is the

battery capacity in Ah, and $I_{loadAVG}$ is the filtered value of the load current, representing the short-term average, which is defined by

$$I_{loadAVG} = I'_{loadAVG} * (1 - \beta) + I_{load}\beta, \quad (3)$$

where $I_{loadAVG}{}'$ is the value from the previous sample and β is the forgetting factor with the value of 5×10^{-5}. The $I_{loadAVG}$ is used for SOC thresholds and for power set-point calculations to prevent fast variations of the calculated values, especially as all loads switch on/off instantly.

On the other side, the actual upper SOC threshold is decreased from the nominal value to prevent overcharging during the time needed for the FP/FC system to lower the power level from the actual to minimum, that is, to the operation level when shutdown can be initiated. The value is calculated by

$$SOC_{MAXact} = SOC_{MAX} - \left(\frac{P_{act}+P_{min}}{2\,U_{batt0}} - I_{loadAVG}\right) * \frac{T_{stop}}{C_{batt}} * 100\%, \quad (4)$$

where P_{act} and P_{min} are the actual and minimum APU power values and T_{stop} is the shutdown time.

3.3 The APU power control

The APU output power is mainly a factor of charging or discharging the battery and serving the average load. Additionally, the APU power is subject to following constraints:

- Maximal and minimal power levels imposed by FP/FC system
- The power transition rate imposed by FP
- Maximal charging current imposed by battery.

These constraints are implemented in the control algorithm, which defines the stack current set point. In the *operation* state the latter is subject to two limitations: the first is the maximal APU output and the second is the maximal battery charging current. Therefore, the following function is used to define it:

$$i_{stack_{ref}} = \min\left(i_{stack_{max_{APU}}}, i_{stack_{max_{BATT}}}\right), \quad (5)$$

with the stack current being limited by the smaller of the APU and battery limitations

$$i_{stack_{max_{APU}}} = \frac{i_{max_{APU}} \cdot U_{batt_0}}{U_{stack_{maxPow}}} \quad \text{and} \quad i_{stack_{max_{BATT}}} = \frac{\left(i_{max_{BATT}} + i_{loadAVG}\right) \cdot U_{batt_0}}{U_{stack_{maxPow}}}, \quad (6)$$

where U_{batt_0} is the nominal battery voltage, $i_{max_{BATT}}$ is maximal battery charging current, and $U_{stack_{maxPow}}$ is the stack voltage at maximal power.

4 APU loads

To analyse the APU operation, the possible loads have to be selected and their profile specified. The electrical loads to be used by the truck driver during the overnight stop are listed

in Table 3, together with their estimated power consumption per single on time night stop, the length of which was estimated to 8.25 hours. In Figure 8 the simulated load profiles for a summer night stop are presented with the total consumption profile in Figure 9. In the winter scenario the air conditioner is replaced by a heater of the same power, which operates for approximately twice as long.

Table 3. Loads of the truck onboard APU

Load type	*Power usage sim (W)*	*Up-time/night sim (h)*	*Energy/night sim (Wh)*
Cooker	*1000*	*0.33*	*330*
Refrigerator	*30*	*8.25*	*240*
Lights	*100*	*3.00*	*300*
Microwave	*800*	*0.33*	*250*
Air conditioner	*1000*	*(16%) 1.33*	*1330*[a]
Heater	*1000*	*(29%) 2.40*	*2400*[a]
Radio or TV	*50*	*3.20*	*160*
Laptop PC	*90*	*3.20*	*280*

[a] An air conditioner is used in the summer scenario and a heater in the winter scenario.

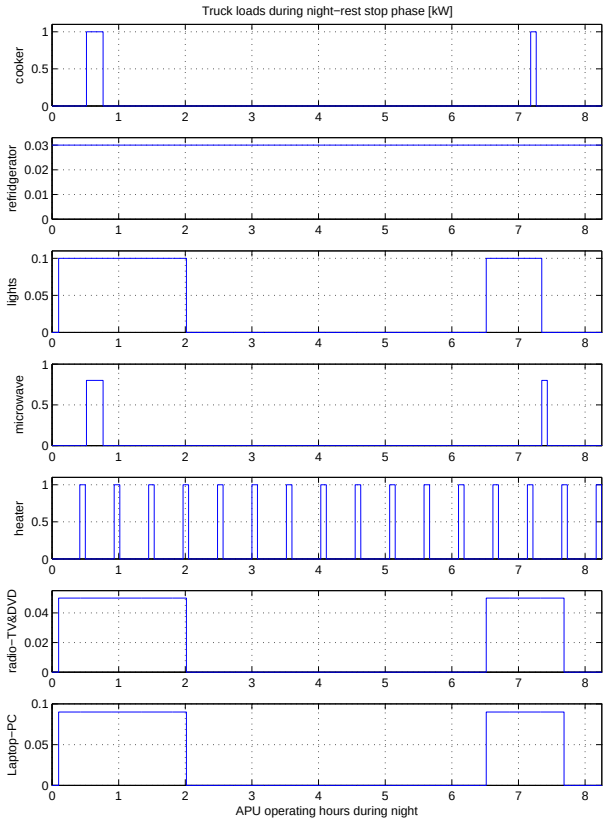

Figure 8. Truck night-stop loads and respective power consumption profile for summer scenario.

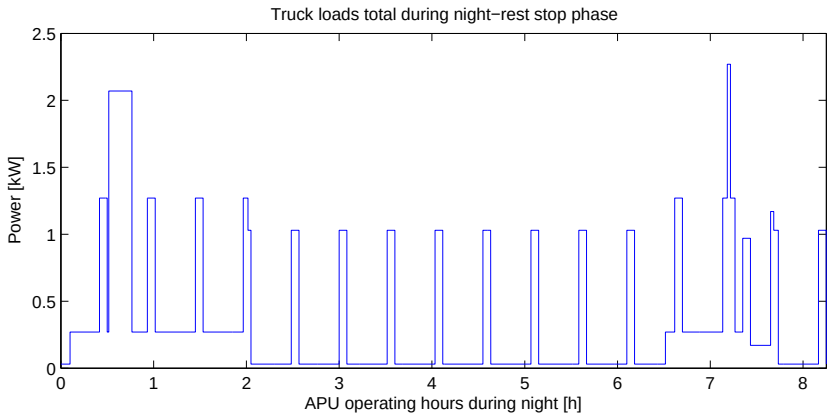

Figure 9. Truck night-stop total power consumption profile for summer scenario.

The night-stop energy consumption of the truck loads amounted to 2.89 kWh during the summer and 3.95 kWh during the winter. Presuming a single APU operation per night, another 0.52 kWh consumed by start-up/shut-down has to be added to that number.

5 Simulations

The simulations considered the following daily scenario:

- The truck stops in the evening with the APU battery filled to 100%, from which all the night-stop electric loads are supplied.
- At the end of the stop, when the main engine is started, the APU must be in *standby*, or be put to s*hutdown* (fuel cutoff) if in operation.
- The APU battery is refilled to 100% during driving by the truck alternator, as in the project scope the APU cannot be operated during driving.

5.1 Experiments with standard truck starting using a lead-acid battery (SLI) with 24V, 220Ah

The simplest and most straightforward way is to use original 24V truck's starting battery. The battery has 220Ah of rated capacity (i.e., 5.280 kWh). With the SOC active range of SLI limited to 70–100%, this results in an operating capacity of 1.584 kWh. Furthermore, to mimic SLI behaviour, the charging current also has to be limited within the control algorithm to 44 A, the maximal allowed charging current for this type of battery (see Table 1). The data of interest from the simulation experiments for the summer and winter scenarios are presented in Figures 10 and 11, respectively.

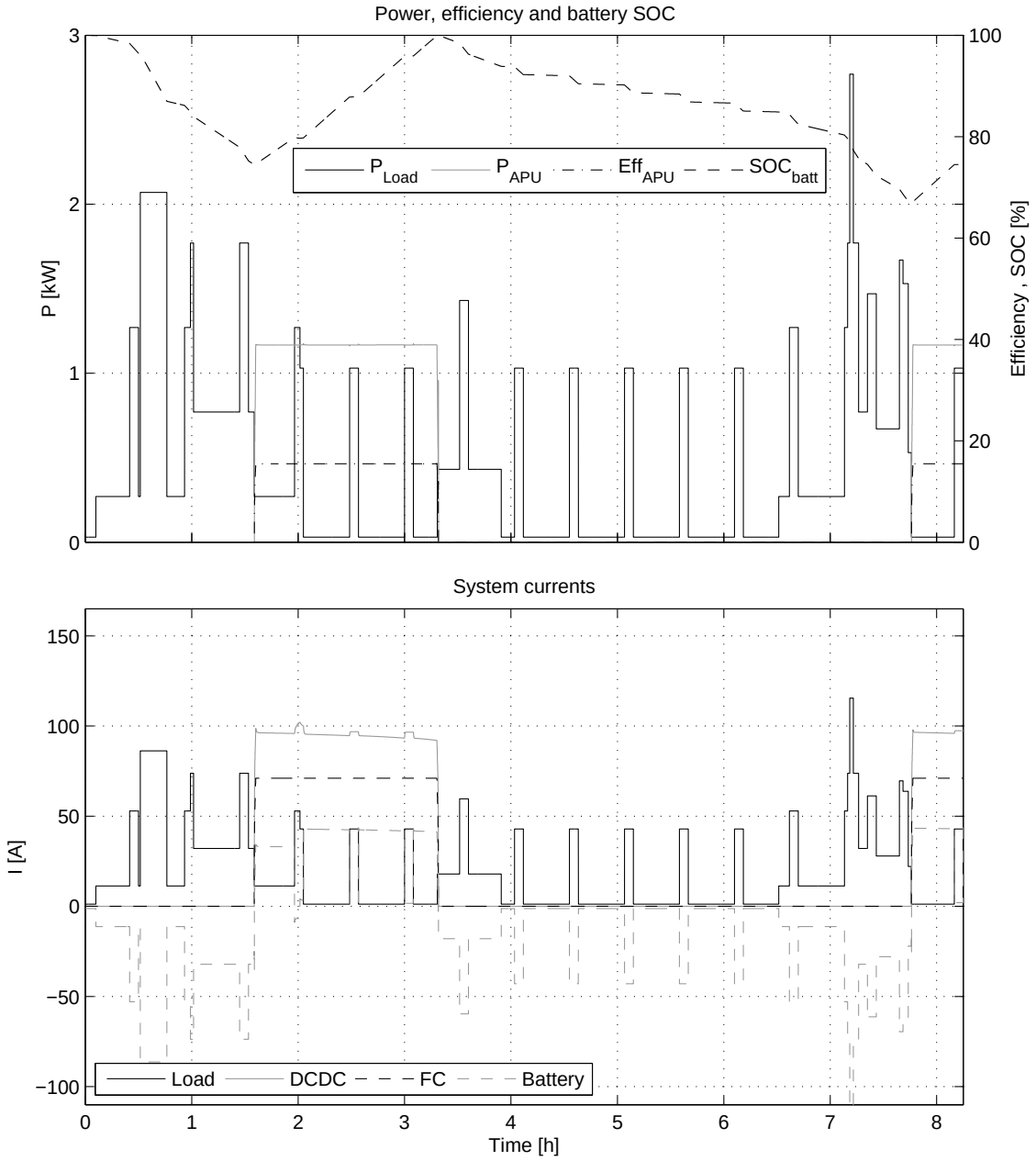

Figure 10. Time plots of summer night-stop simulation using 220 Ah SLI battery; the upper chart presents the APU (grey) and load (black) power on the left-hand scale and the APU efficiency (dash-dotted) and battery SOC (dashed) on the right-hand scale. The bottom chart presents the time plots of the system currents: load (black), DCDC in (grey), FC stack (black, dashed) and battery (grey, dashed).

Several observations can be made. First, due to the low value of the allowed charging current related to the lead-acid batteries, the APU in general only operated at 50% of the rated level, which leads to lower APU operational efficiency. Second, even in summer the small battery buffer results in the need for a second starting of the APU during the single stop – this (a) further decreases the overall efficiency due to the energy consumed by an additional startup and shutdown and (b) doubles the number of APU starts, which affects its lifetime. Third, the relatively high discharge current also affects the SLI battery lifetime. However, in the winter experiment (Figure 11) the battery is close to full at the end of the simulation, which exploits the APU's efficiency advantage over the truck's alternator. Another phenomenon can be

observed in Figure 10: the SOC falls slightly below 70 % at time of 7.65h as the load consumption during APU startup is higher than the estimated (one can notice high load values and spikes from 7h onwards).

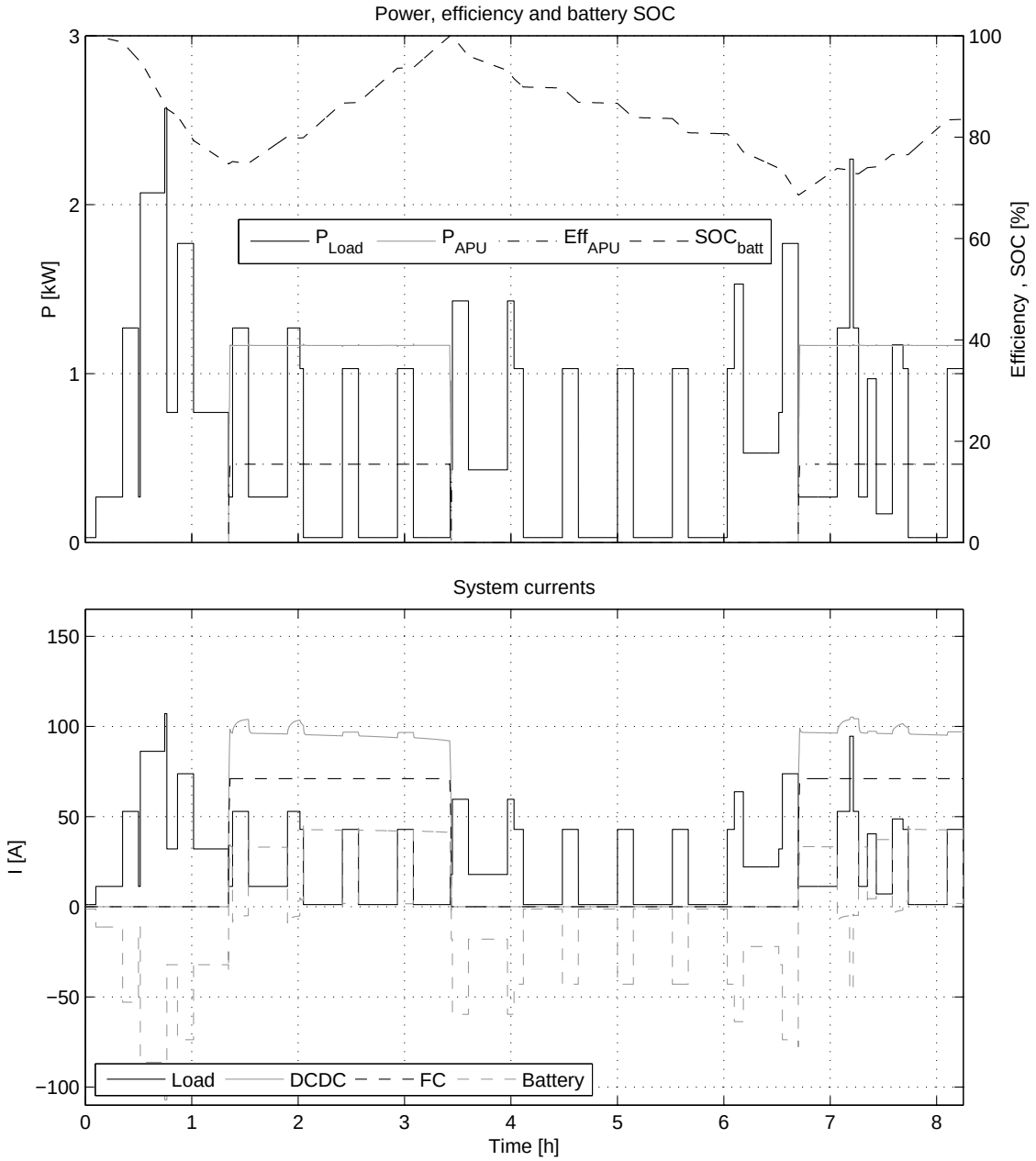

Figure 11. Time plots of winter night-stop simulation using 220 Ah SLI battery. Signals as in Figure 10.

5.2 Experiments with lead-acid traction battery with 24V, 220 Ah

This battery has the same rated capacity as the SLI in the previous case (220 Ah). However, the traction battery has an active SOC range between 20% and 100%, which represents an operating capacity of 4.224 kWh. The experiment plots are presented in Figures 12 and 13.

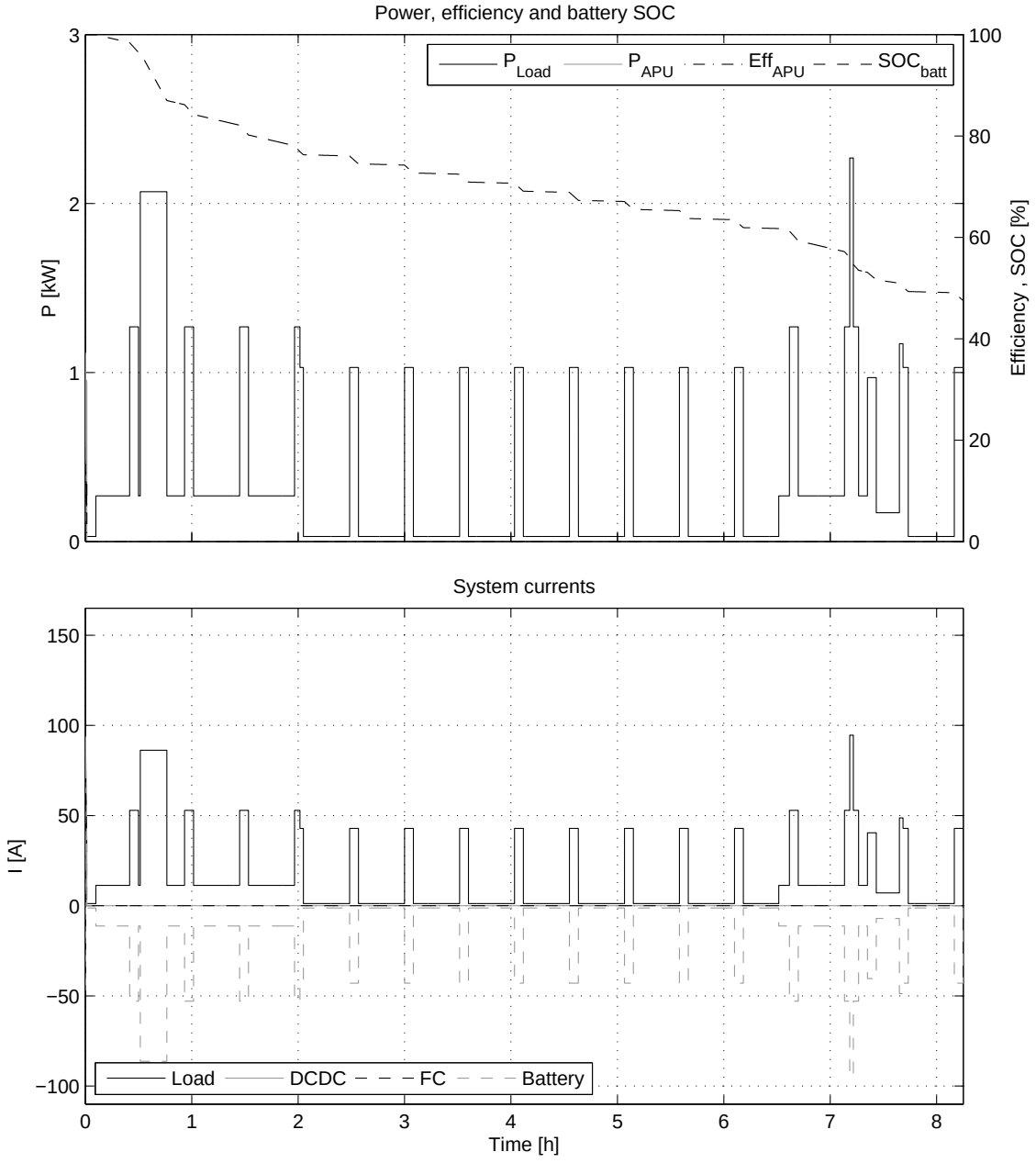

Figure 12. Time plots of summer night-stop simulation using 220 Ah Traction battery. Signals as in Figure 10.

In the summer case, the battery suffices for the whole night-stop consumption, while in the winter scenario the APU is engaged towards the end of the night stop, only managing to fill the battery by 10%. The traction battery has two main downsides: first it is not capable of providing power for engine starting, and the second is again the low charging current limitation leading to the APU operating at lower efficiency, the same as is the case with the SLI battery from the previous experiment. The degradation of the discharge current is somewhat less strongly expressed, but is still an issue.

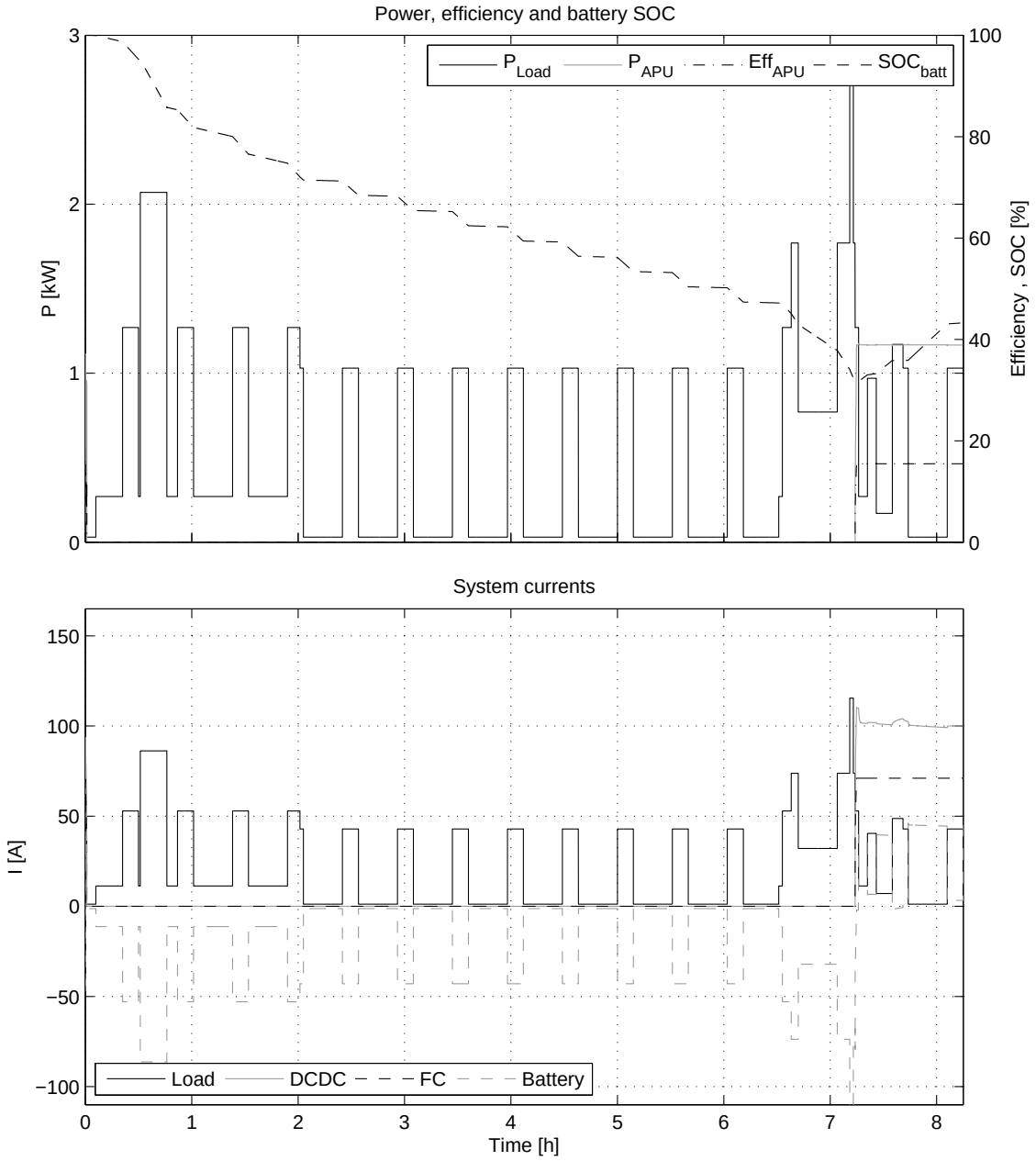

Figure 13. Time plots of winter night-stop simulation using 220 Ah traction battery. Signals as in Figure 10.

5.3 Experiments with Li-ion starting-capable battery with 26V, 100Ah

The lithium battery has a rated capacity of 100 Ah; it has an active SOC range of between 10% and 100%, which results in its operation with 90 Ah of rated capacity (i.e., 2.340 kWh). The charging current of 100 A and above is not a limitation to this type of battery. The experiment plots are presented in Figures 14 and 15.

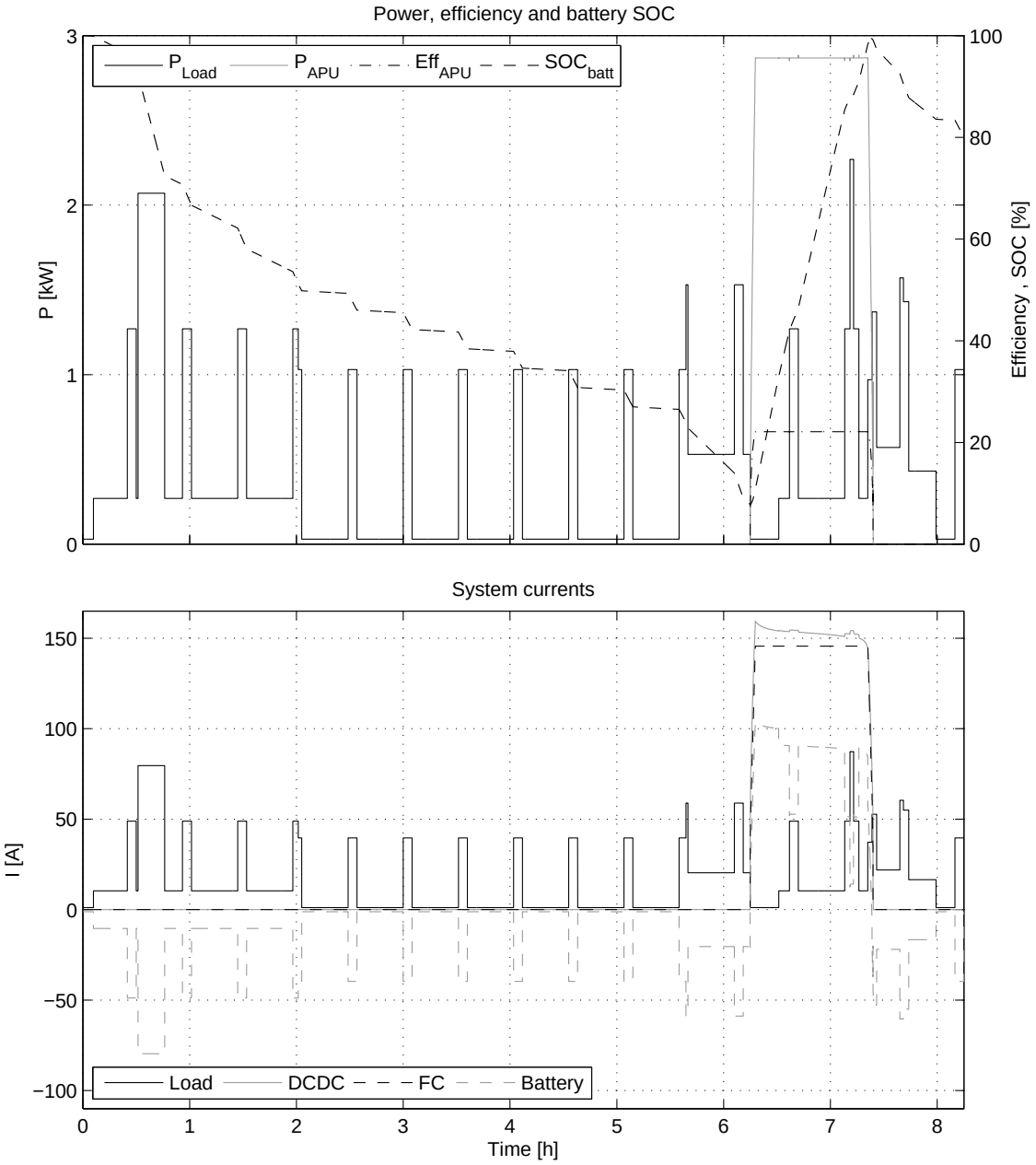

Figure 14. Time plots of summer night-stop simulation using 100 Ah Li-Ion battery. Signals as in Figure 10.

The summer simulation experiment shows that the lithium battery has enough capacity to avoid the need for second APU startup, and has still plenty of power available for starting the main engine at the end of the stay. It also allows the APU to run close to the rated power, where it has the highest efficiency. In the winter scenario the battery is still sufficient to prevent a second APU run, but as a consequence a lot of energy is required to fill up the battery from the low-efficiency truck alternator after the night stop.

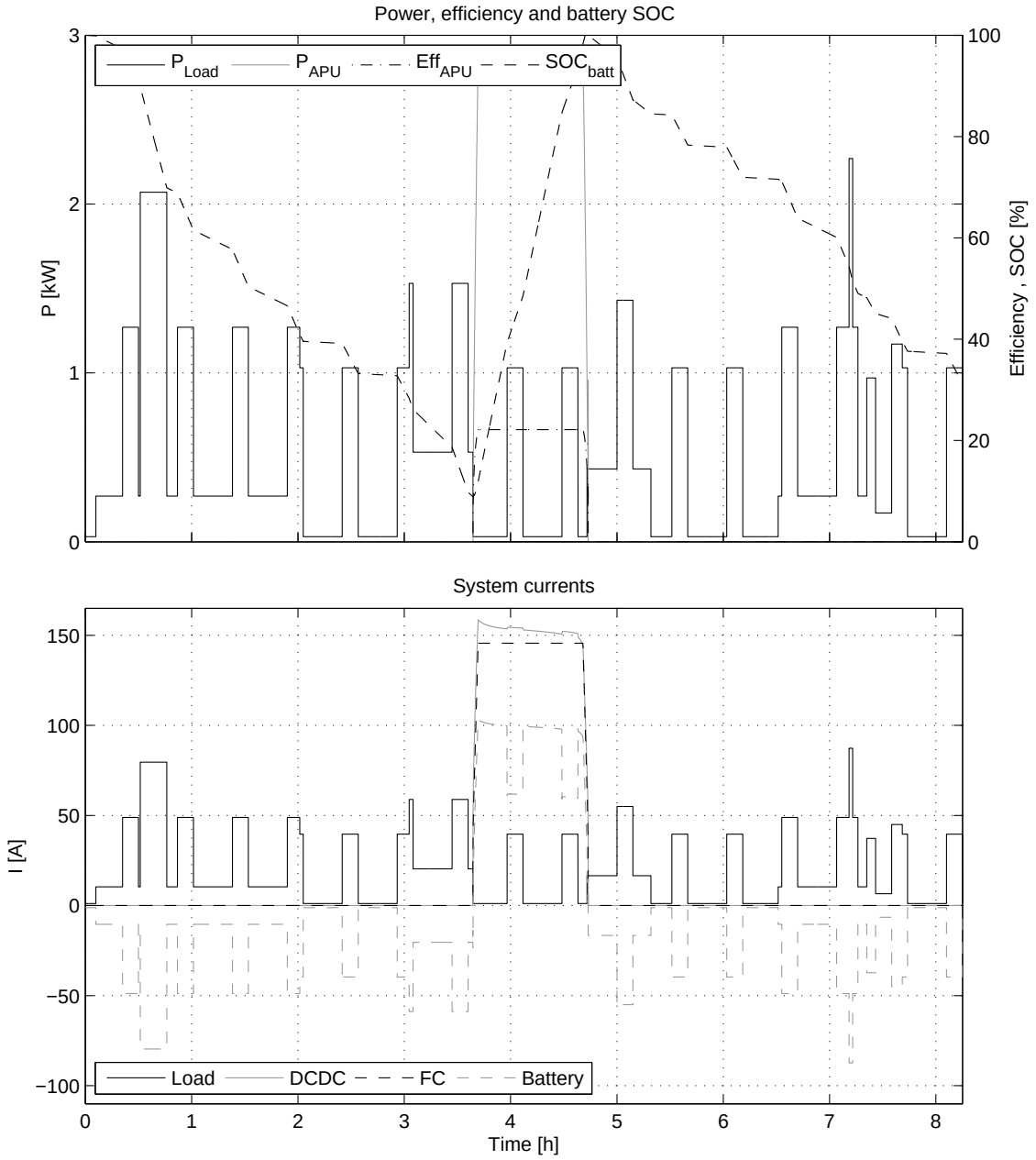

Figure 15. Time plots of winter night-stop simulation using 100 Ah Li-Ion battery. Signals as in Figure 10.

6 Evaluation criteria and analysis

Further insight into the battery charge and discharge process and APU operation can be obtained from simulations of the complete model using the specified load profiles for the discussed three batteries. The APU power distribution scheme throughout the system is presented in Figure 16. Basically, the overall system's input/output efficiency can be calculated from:

$$\mu_{APU} = \mu_{FP}\mu_{FC}\mu_{DCDC}\mu_{BoP}, \tag{7}$$

where μ_{FP}, μ_{FC}, and μ_{DCDC} are the stack, fuel processor and power converter efficiencies from the characteristics given in Figures 2 and 4, and μ_{BoP} is the electric efficiency including the BoP

components' power consumption. However, this calculation is only valid for the APU *operation* state, as it disregards the startup and shutdown phases.

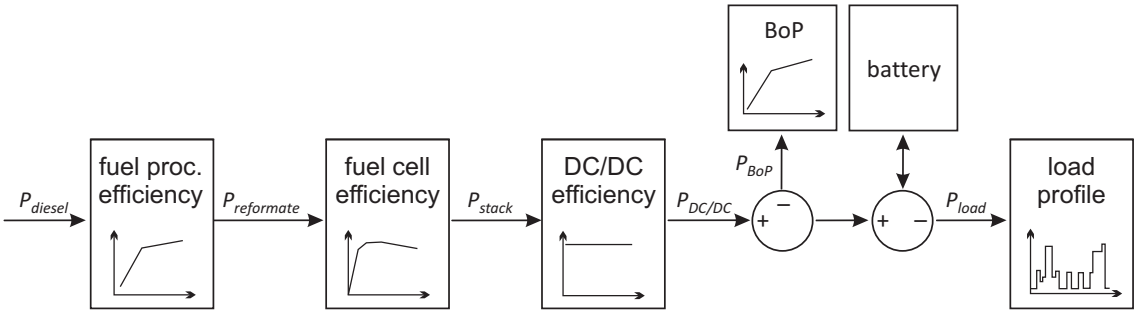

Figure 16. The APU main component efficiencies and power flow.

To obtain the overall position on efficiency, the input and output power have to be assessed over the whole simulation period and beyond. The APU output power is easy to integrate over the time, while the input (fuel) power is somewhat more difficult to calculate, as the batteries are not equally full after 8.25 hours of simulation. In case the APU is running when the night stop ends, shutdown has to be initiated at that time and the respective energy has to be accounted for. To even up the experiments, we assumed that all batteries were filled back to 100% during the truck driving after the stop. During driving the electricity production efficiency μ_{ICEel} was estimated to be 10% (average engine efficiency of 20% and alternator efficiency of 50%). The total fuel energy is then obtained by

$$E_{fuel} = \int_0^{8.25} P_{fuelAPU}\,dt + \frac{\left[\int_{t_{night\ end}}^{t_{batt\ full}} P_{batt\_fill}\,dt + E_{stop}\right]}{\mu_{ICEel}}, \quad (8)$$

where $P_{fuelAPU}$ is the power of flow of the diesel consumed by the APU, P_{batt_fill} is the battery charging power from the truck alternator, $t_{night\ end}$ is the time at the end of night stop, $t_{batt\ full}$ is the time when battery is filled back to 100%, and E_{stop} is the energy consumed during APU shutdown phase. The efficiency of the night-stop electricity production is then defined as the ratio of the energy required by truck loads and total fuel energy consumed by both APU and truck engine (8) as

$$\mu = \frac{E_{load}}{E_{fuel}}, \quad (9)$$

where E_{fuel} is the energy of the total fuel consumed (by both APU and truck engine) to produce the electricity for the night stop. The criteria values for the experiments with all batteries are given in Table 4.

Table 4. Energy consumption calculations

Battery type	*Energy delivered by APU*	*Energy of diesel consumed by APU*	*Operational efficiency of the APU*	*Energy required to fill up battery*	*Energy of diesel consumed by truck engine*[*]	*Total diesel energy consumed*	*Total night-stop efficiency*
			Summer scenario truck load consumption = 2.89 kWh				
SLI	*2.57 kWh*	*17.04 kWh*	*15.4%*	*1.56 kWh*	*18.0 kWh*	*35.1 kWh*	*8.2%*
Traction	*0*	*0*	*/*	*3.18 kWh*	*31.8 kWh*	*31.8 kWh*	*9.1%*
Lithium	*3.19 kWh*	*14.93 kWh*	*21.7%*	*0.59 kWh*	*5.9 kWh*	*20.8 kWh*	*13.9%*
			Winter scenario *truck load consumption = 3.95 kWh*				
SLI	*4.23 kWh*	*27.81 kWh*	*15.4%*	*1.02 kWh*	*12.6 kWh*	*40.4 kWh*	*9.8%*
Traction	*1.19 kWh*	*8.1049 kWh*	*15.4%*	*3.43 kWh*	*34.3 kWh*	*44.8 kWh*	*8.8%*
Lithium	*2.99 kWh*	*14.05 kWh*	*21.7%*	*1.98 kWh*	*19.8 kWh*	*33.9 kWh*	*11.7%*

[*]Energy consumed by diesel engine to fill the battery and provide power for shutdown in case the APU was running when night-stay ended, or remaining time of shutdown procedure in case it was already initiated.

7 Discussion

Due the fact that the APU is currently under development and the model somewhat differs from the real system, the values should be taken carefully. However, the study experience and insight in operation are already useful for informed selection of the most appropriate battery. With reference to the simulation plots and performance data in Table 4, the following remarks can be made:

1. One of the main problems of the lead-acid batteries is the discharge current capability, which drastically limits their use or impose unacceptably high restrictions on minimum battery size (cca 400 Ah) – almost double of what is available here. Additionally the traction battery is not able to provide current required for engine start.
2. The APU operational efficiency with the lithium-ion battery is approximately 50% higher than with lead-acid. This is predominantly due to the much higher charging current capability of the lithium batteries compared to lead-acid batteries resulting in APU running at higher operating point with higher efficiency (lower relative BoP losses and higher H_2 utilization). With the available battery sizes the charging current limitation of the lead-acid batteries favors APUs with approximately halved nominal power level.
3. Due to battery charging efficiency, and added startup/shutdown consumption, the net overall efficiencies are lower than the operational values.
4. If the APU is operating during the time when a larger load is active, as is the case in winter SLI and summer lithium battery experiments (Figures 10 and 13), the resulting

overall efficiency is higher. This is because the APU consequentially operates for a longer time and provides more energy with higher efficiency compared to truck engine.

5. In the summer case, the 220 Ah traction battery can provide energy for the whole night, but it has to be filled by the truck alternator with less efficiency; on the other hand, it does not require the APU startup and shutdown energy.
6. The size of the lithium battery makes it most suitable for summertime load but rather small for the winter, when it consequentially ends the night stop with low a SOC value that requires a lot of energy from the alternator to fill-up. Still, in both cases the lithium battery yields the highest overall efficiency, thanks to its much higher operational efficiency, which results in a saving of notable amount of energy (i.e. diesel) compared to the other two types, especially on the longer term.
7. The overall efficiency values are about double than the truck-engine idling electricity production (efficiency ca 5%), but not so much when compared to a small dedicated power generator. However, (i) the exhaust gasses of the APU are much cleaner, as the close to 100% conversion of all HC components in the diesel is achieved and the sulphur and CO are removed within the cleanup reactors and (ii) the sound level (below 60 dB) during operation is considerably lower compared to either truck engine or diesel generator of required power level (70-80 dB).

At this point it is important to note that the FCGEN is a research project with the goal of developing, tuning, and integrating the latest technology components and demonstrating their use on the truck. For the BoP components the market has been searched and best compromises were taken, but they still consume very large part of the produced electricity. Yet, the power level matching of all components and reactors and the optimization of overall efficiency would represent a comprehensive task that belongs to the later steps of the technology deployment process, which is out of scope of this project. As a consequence, this system requires a highly versatile energy buffer and its efficiency levels are quite low. Therefore, the lithium battery yields the highest efficiency and copes best with the task degradation-wise, but comes with the high price of lithium technology. However, by taking the steps to further optimize the APU process component- and control-wise, to significantly lower the BoP consumption and shorten the startup time, the operational efficiency can be notably improved to above 30 % and the battery requirements eased down.

In the field of the truck APUs also the Solid Oxide fuel cell (SOFC) is the competing technology [24]. There the whole APU process and its controls are not as complex as the one presented here, whereas the efficiencies for the optimized systems are comparable. However, due to high operating temperatures, with SOFC one of the main issues is long startup (preheat) time, which imposes even higher requirements for the battery capacity.

8 Conclusion

In the present study, we have introduced a model-based approach to battery evaluation for a truck anti-idling application for a diesel-powered PEM FC-based APU, currently being developed within the FCGEN EU project. This approach can also be applied to other case studies (yachting, the household, etc.) with other components (SOFC, etc.) and operating requirements without substantial effort.

Beside the fact that the battery is an essential part of the APU, and helps to unlock its full potential, the study results also indicate that the necessary preconditions for this is the appropriate dimensioning of all components within the APU, as well as the alignment of the nominal APU power and the battery with the targeted load demand.

The main findings of the study stem from the fact that the depending on size and type, batteries impose different current limitations. From the charging aspect the APU nominal power has to be targeted at maximal charging current of the battery. On the other hand the battery also limits the load which can be at maximum the sum of discharge power (current) and APU power. In the presented case this calls for double size of lead-acid the battery or halved power of the APU, while the lithium battery is quite closely matched with APU power, only a bit underpowered for winter load. The latter also imposes less weight and volume issues.

To this point the FC-based APUs already represent an interesting option for certain application niches. However, by further improving the overall system from component, technology and control aspect and this way pushing the efficiency, cost, and durability boundaries further, such systems have a certain future in this and other industrial and domestic application fields.

Acknowledgement

The research leading to these results has received funding from the European Union's Seventh Framework Program (FP7/2007-2013) for the Fuel Cells and Hydrogen Joint Technology Initiative under grant agreement no. [277844], from the Slovenian Research Agency through the Research Programme P2-0001, and from the *Low-carbon Technologies Centre of Excellence* (CO NOT) financed by the Ministry of Higher Education, Science and Technology, and co-financed by the European Regional Development Fund.

References

[1] Barbir, F. (2005). PEM Fuel Cells: Theory and Practice. Elsevier/Academic Press, Burlington, (ISBN 978-0-12-078142-3).

[2] Srinivasan, S. (2006). Fuel cells: From Fundamentals to Applications. Springer Science-Business Media LLC.

[3] Sammes, N. (2006). Fuel Cell Technology. Springer Verlag, London.

[4] Jovan, V., Perne, M., Petrovčič, J. (2010). An assessment of the energetic flows in a commercial PEM fuel-cell system. Energy Conversion and Management, 51, 2467–2472.

[5] Lee J. S., Quan N. D., Hwang J. M., Lee S. D., Kim H., Lee H., Kim H. S. (2005). Polymer electrolyte membranes for fuel cells. Journal of Industrial and Engineering Chemistry, 12(2), 175–183.

[6] Ramos-Paja, C. A., Bordons C., Romero A., Giral R., Martínez-Salamero L. (2009). Minimum fuel consumption strategy for PEM fuel cells. IEEE Transactions on industrial electronics, 56(3), 685–696.

[7] Silva, S. B., Severino, M. M., de Oliveira, M. A. G. (2013). A stand-alone hybrid photovoltaic, fuel cell and battery system: A case study of Tocantins, Brazil. Renewable Energy, 57, 384–389.

[8] Barelli, L., Bidini, G., Ottaviano, A. (2012). Optimization of a PEMFC/battery pack power system for a bus application. Applied Energy, 97, 777–784.

[9] Vasallo, M.,J., Bravo, J.M., Andújar, J.M. (2013). Optimal sizing for UPS systems based on batteries and/or fuel cell, Applied Energy, 105, 170–181.

[10] Debenjak, A., Boškoski, P., Musizza, B., Petrovčič, J., Juričić, Đ. (2014). Fast measurement of proton exchange membrane fuel cell impedance based on pseudo-random binary sequence perturbation signals and continuous wavelet transform. Journal of Power Sources, 254, 112–118.

[11] Boškoski, P., Debenjak, A. (2014). Optimal selection of proton exchange membrane fuel cell condition monitoring thresholds, Journal of Power Sources, 268, 692-699.

[12] Agnolucci, P. (2007). Prospects of fuel cell auxiliary power units in the civil markets. International Journal of Hydrogen Energy, 32(17), 4306–4318.

[13] Engelhardt, P., Maximini, M., Beckmann, F., Brenner, M. (2012). Integrated fuel cell APU based on a compact steam reformer for diesel and a PEMFC. International Journal of Hydrogen Energy, 37(18), 13470–13477.

[14] Severin, C., Pischinger, S., Ogrzewalla, J. (2005). Compact gasoline fuel processor for passenger vehicle APU. Journal of Power Sources, 145(2), 675–682.

[15] Aicher, T., Lenz, B., Gschnell, F., Groos, U., Federici, F., Caprile, L., Parodi, L. (2006). Fuel processors for fuel cell APU applications. Journal of Power Sources, 154(2), 503–508.

[16] Rahman, S. M. A., Masjuki, H. H., Kalam, M. A., Abedin, M. J., Sanjid, A., Sajjad, H. (2013). Impact of idling on fuel consumption and exhaust emissions and available idle-reduction technologies for diesel vehicles: A review. Energy Conversion and Management, 74, 171–182.

[17] Lim h. (2002). Study of Exhaust Emissions from Idling Heavy-Duty Diesel Trucks and Commercially Available Idle-Reducing Devices. United States Environmental Protection Agency.

[18] Stanich, D. (2008). Commercial diesel vehicle owners warned of idling restrictions. News Release. Californian Environmental Protection Agency. Available at: http://www.arb.ca.gov/newsrel/nr100908.htm

[19] Jain, S., Chen, H.-Y., Schwank, J. (2006). Techno-economic analysis of fuel cell auxiliary power units as alternative to idling. Journal of Power Sources, 160(1), 474–484.

[20] Lutsey, N., Brodrick C.-J., Lipman, T. (2007). Analysis of potential fuel consumption and emissions reductions from fuel cell auxiliary power units (APUs) in long-haul trucks. Energy, 32(12), 2428–2438.

[21] Contestabile, M. (2010). Analysis of the market for diesel PEM fuel cell auxiliary power units onboard long-haul trucks and of its implications for the large-scale adoption of PEM FCs. Energy Policy, 38(10), 5320–5334.

[22] Brodrick, C. -J., Lipman, T. E., Farshchi, M., Lutsey, N. P., Dwyer, H. A., Sperling, D., Gouse, III, S. W., Harris, D. B., King, F. G. (2002). Evaluation of fuel cell auxiliary power units for heavy-duty diesel trucks. Transportation Research Part D: Transport and Environment, 7(4), 303–315.

[23] FCGEN (Fuel Cell Based On-board Power Generation) (2011). FCH JU European project. Available at: http://www.fch-ju.eu/project/fuel-cell-based-board-power-generation

[24] DESTA project to demonstrate European SOFC truck APU (2012). Fuel Cells Bulletin, 5, p. 4.

[25] Barelli, L., Bidini, G., Ottaviano, A. (2012). Optimization of a PEMFC/battery pack power system for a bus application. Applied Energy, 97, 777–784.

[26] Leadbetter, J., Swan, L. G. (2012). Selection of battery technology to support grid-integrated renewable electricity. Journal of Power Sources, 216, 376–386.

[27] Pregelj, B., Vrečko, D., Jovan, V. (2011). Improving the operation of a fuel-cell power unit with supervision control: A simulation study. Journal of Power Sources, 196(22), 9419–9428.

[28] Pasel, J. , Samsun, R. C., Peters, R., Stolten, D. (2013). Fuel processing of diesel fuel and kerosene for auxiliary power unit applications. Energy and Fuels, 27, 4386–4394.

[29] Samsun, R.C., Pasel, J., Janßen, H., Lehnert, W., Peters, P., Stolten, D., (2014). Design and test of a 5 kWe high-temperature polymer electrolyte fuel cell system operated with diesel and kerosene, Applied Energy, 114, 238-249.

[30] S1 Fuel Cell Data Sheet, Powercell AB (no date). Available at: http://www.powercell.se/wp-content/uploads/2010/09/Datasheet_FuelCell-rev-100909.pdf

[31] Mathworks, MATLAB/Simulink/SimPowerSystems/Battery model, http://www.mathworks.com/help/physmod/sps/powersys/ref/battery.html.

[32] Reinout Vader (2007). Energy Unlimited: The Book. Revision 9. Victron Energy B.V.

[33] Qualion battery specification (no date). Available at: http://www.quallion.com/images-pdf/24V-%20QLD0100-MT.pdf

[34] Crompton, T. R. (2000). Battery Reference Book. 3rd ed. Reed Educational and Professional Publishing Ltd, Oxford.